Eur. J. Mineral.
2005, **17**, 749-759

Ferrorosemaryite, $NaFe^{2+}Fe^{3+}Al(PO_4)_3$, a new phosphate mineral from the Rubindi pegmatite, Rwanda

FRÉDÉRIC HATERT[1,*], PIERRE LEFÈVRE[1], ANDRÉ-MATHIEU FRANSOLET[1], MARIE-ROSE SPIRLET[2], LEILA REBBOUH[2], FRANÇOIS FONTAN[3] and PAUL KELLER[4]

[1]Laboratoire de Minéralogie, Département de Géologie, Université de Liège, Bâtiment B.18, B-4000 Liège, Belgium
[2]Département de Physique, Bâtiment B.5, Université de Liège, B-4000 Liège, Belgium
[3]Laboratoire de Minéralogie, LMTG-UMR 5563, Observatoire Midi Pyrénées, 14 Avenue E. Belin, F-31400 Toulouse, France
[4]Institut für Mineralogie und Kristallchemie, Universität Stuttgart, Pfaffenwaldring 55, D-70569 Stuttgart, Germany

Abstract: Ferrorosemaryite, ideally $\square NaFe^{2+}Fe^{3+}Al(PO_4)_3$, is a new mineral species from the Rubindi pegmatite, Rwanda. It occurs as large idiomorphic grains reaching 3 mm, embedded in scorzalite. Associated phosphate minerals are scorzalite, trolleite, montebrasite, bertossaite, brazilianite, with accessory augelite, triplite and lacroixite. The mineral is transparent and exhibits a dark-green to bronze colour, with a resinous lustre and with a greenish to brownish streak. It is non-fluorescent, brittle, and shows a perfect {010} cleavage and a good $\{\bar{1}01\}$ cleavage. The estimated Mohs hardness is 4. The calculated density is 3.62 g/cm^3. Ferrorosemaryite is biaxial negative, with $\alpha = 1.730(5)$, $\beta = 1.758(7)$, and $\gamma = 1.775(5)$ ($\lambda = 590$ nm). Pleochroism is from dark green (X) to dark brown (Z). The measured $2V$ angle is 82(1)°, and the calculated $2V$ angle is 75°. A strong dispersion r < v has been observed, but the optical orientation has not been determined. Electron microprobe analyses gave P_2O_5 46.00, Al_2O_3 9.12, Fe_2O_3 21.01, FeO 11.10, MgO 0.19, MnO 7.96, CaO 0.44, Na_2O 2.85, K_2O 0.01, total 98.68 wt. %. The resulting empirical formula, calculated on the basis of 12 O, is $\square_{1.00}(Na_{0.42}Mn^{2+}_{0.28}Ca_{0.04}\square_{0.26})_{\Sigma 1.00}(Fe^{2+}_{0.71}Mn^{2+}_{0.24}Fe^{3+}_{0.05})_{\Sigma 1.00}Fe^{3+}_{1.00}(Al_{0.82}Fe^{3+}_{0.16}Mg_{0.02})_{\Sigma 1.00}[(P_{0.99}\square_{0.01})O_4]_3$. The single-crystal unit-cell parameters are $a = 11.838(1)$, $b = 12.347(1)$, $c = 6.2973(6)$ Å, $\beta = 114.353(6)°$, and $V = 838.5(1)$ Å^3, space group $P2_1/n$. The eight strongest lines in the powder X-ray diffraction pattern [d(in Å)(I)(hkl)] are: 8.102(30)(110), 6.167(50)(020), 5.382(40)(200), 4.054(45)(220), 3.448(65)(310), 3.011(40)$(11\bar{2})$, 2.693(75)(400), 2.677(100)(240). Ferrorosemaryite is the Fe^{2+} analogue of rosemaryite, and belongs to the wyllieite group of minerals. The crystal structure of ferrorosemaryite has been refined, based on single-crystal X-ray diffraction data, to $R_1 = 2.43$ %. The infrared spectrum is similar to those of alluaudite-type phosphates. The mineral species and name were approved by the Commission on New Minerals and Mineral Names of the International Mineralogical Association (no. 2003-063).

Key-words: ferrorosemaryite, new phosphate mineral, wyllieite group, crystal structure, Rubindi pegmatite, Rwanda.

Introduction

Among the four valid type-minerals reported in Rwanda, three were described in the Buranga pegmatite, which is host to over hundred of other mineral species (Daltry & Von Knorring, 1998). More than half of the recorded minerals from Buranga are phosphates, of which two compositional groups are recognised: Al-dominant and Fe-Mn-dominant phases (Von Knorring, 1970). Whereas the phosphate mineralogy of the Buranga pegmatite is relatively well known, detailed descriptions of phosphate mineral associations occurring in other granitic pegmatites from the Gatumba field are not really abundant. In order to complete the mineralogical description of these associations and to discuss their petrography, Lefèvre (2003) thoroughly investigated several samples collected in the Rubindi-Kabilizi pegmatites by A.-M. F., F.F. and P.K. in 1983. These samples contained aluminum phosphates, mostly montebrasite and scorzalite, with bertossaite, brazilianite, and trolleite.

Embedded in a few scorzalite-rich samples from Rubindi, a dark green mineral was observed. A preliminary examination under the polarizing microscope and by powder X-ray diffraction indicated that this mineral belongs to the alluaudite or wyllieite group of minerals. The electron microprobe analyses indicated the presence of aluminium in significant amounts, thus confirming the identification of a wyllieite-type phosphate. The $P2_1/n$ space group of wyllieite was furthermore confirmed by Weissenberg photographs.

This mineral corresponds to the Fe^{2+}-rich equivalent of rosemaryite, *i.e.* $\square NaFe^{2+}Fe^{3+}Al(PO_4)_3$, not yet described.

*E-mail: fhatert@ulg.ac.be

0935-1221/05/0017-0749 $ 4.95
DOI: 10.1127/0935-1221/2005/0017-0749

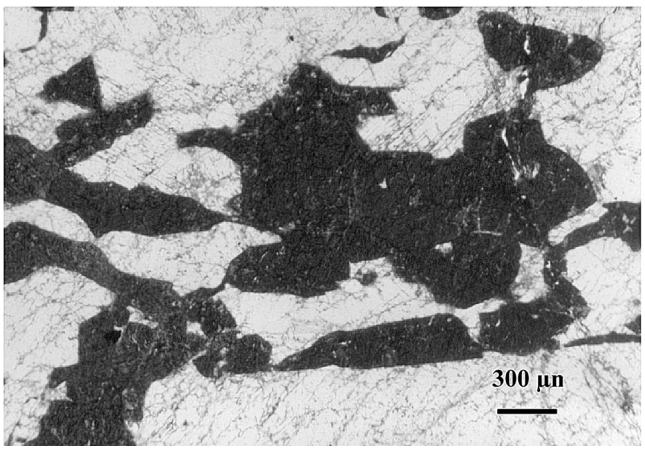

Fig. 1. Large grains of ferrorosemaryite (black), included in scorzalite from Rubindi, Rwanda.

The mineral is named ferrorosemaryite, in accordance with the nomenclature of the wyllieite group (Moore & Ito, 1979) and with the IMA-CNMMN rules. The mineral species and name were approved by the Commission on New Minerals and Mineral Names of the International Mineralogical Association (no. 2003-063), and the holotype is stored in the collection of the Laboratory of Mineralogy, University of Liège, Belgium (no. 20326).

Geological setting

The pegmatite of Rubindi-Kabilizi is located 3 km WNW of the Muhororo village, south of the Rubindi river, at about 50 km west of Kigali, Rwanda, in the famous pegmatitic field of Gatumba. As other cassiterite-rich pegmatites of this area reported on the geological map of Rwanda (Ruhengeri sheet S2/29 SE, scale: 1/100.000), the Rubindi-Kabilizi pegmatite crosscuts the dark gray micaschists and quartzites of the Kibuye Formation. The Kibuye Formation corresponds to the upper part of the Pindura Group of Mesoproterozoic age (M. Errera, pers. commun.).

As for many other pegmatitic ore bodies known in the region of Gatumba, no geological description of the Rubindi-Kabilizi pegmatite is given in the literature. Moreover, on the field, virtually nothing remains of the pegmatitic ore body, except an open pit with few remnants of the pegmatite, and barren dumps. This fact is simply due to the small-scale mining activities of the cassiterite and columbite-tantalite ore bodies, frequent in the country during the fifties or the sixties of the past century (see the pictures published by Varlamoff (1975)). About twenty years ago, we (F.F., P.K. and A.M.F.) still observed the same type of mining techniques (Domergue *et al*., 1989).

According to sketchy observations, still possible during the eighties, in the Rubindi mine as well as in the neighbouring Kabilizi mine, south of the same hill, we noticed presence of K-feldspars and of cleavelandite, both deeply altered, among the loose blocks. Besides remnants of the quartz core, we reported masses of quartz, sometimes with fragments of completely kaolinised spodumene crystals. We also found coarsed-grained masses of green mica mixed with quartz similar to the greisens described by Varlamoff (1963) in a general note on the granitic pegmatites of Central Africa. Additionally, among the blocks of quartz or feldspars, striking phosphate associations with a lot of amblygonite-montebrasite caught our attention because they recalled the aluminium-rich phosphate associations already known in Buranga (Von Knorring, 1970) or in Rusororo (Fransolet, 1989), neighbouring pegmatites located at about 6 km east of Rubindi-Kabilizi. These field observations lead us to conclude that Rubindi-Kabilizi was another lithium-rich pegmatite, strongly albitised in the Gatumba field.

Recently, Lefèvre (2003) carefully described the phosphate minerals occurring in these associations. He reported the presence of montebrasite, scorzalite, bertossaite, brazilianite, trolleite, augelite, lacroixite, ferrorosemaryite, and triplite-zwieselite.

Physical properties

Ferrorosemaryite forms large idiomorphic grains reaching 3 mm, embedded in scorzalite (Fig. 1). The mineral is transparent and exhibits a dark-green to bronze colour, with a resinous lustre and with a greenish to brownish streak. It is non-fluorescent, brittle, and shows a perfect {010} cleavage and a good {$\bar{1}$01} cleavage. The estimated Mohs hardness is 4. The density can not be measured because ferrorosemaryite grains are intimately associated with scorzalite; the calculated density is 3.62 g/cm^3. Ferrorosemaryite is biaxial negative, with α = 1.730(5), β = 1.758(7), and γ = 1.775(5) (with λ = 590 nm). Pleochroism is from dark green (*X*) to dark brown (*Z*). The measured 2*V* angle is 82(1)°, and the calculated 2*V* angle is 75°. A strong dispersion r < v has been observed, but the optical orientation has not been determined.

Chemical composition

Quantitative chemical analyses were performed on isolated crystals with a Cameca SX-50 electron microprobe (Université Paul Sabatier, Toulouse, France) operating in the wavelength-dispersion mode, with an accelerating voltage of 15 kV and a beam current of 20 nA. The following standards were used: graftonite (P, Mn), corundum (Al), hematite (Fe), periclase (Mg), wollastonite (Ca), albite (Na) and sanidine (K).

As ferrorosemaryite belongs to the wyllieite group of minerals, according to the single-crystal structure refinement, the chemical formula was calculated on the basis of 12 O (Table 1). Fe^{2+} and Fe^{3+} were calculated according to the interpretation of the Mössbauer spectrum (Fig. 2), which gives 63 % Fe^{3+} and 37 % Fe^{2+}. The presence of both Fe^{2+} and Fe^{3+} is confirmed by the green colour of the mineral, which is caused by charge transfers between Fe^{2+} and Fe^{3+} in the octahedral chains of the atomic structure. The occurrence of Mn^{3+} in ferrorosemaryite can be definitely ruled out, because the oxygen fugacity necessary for

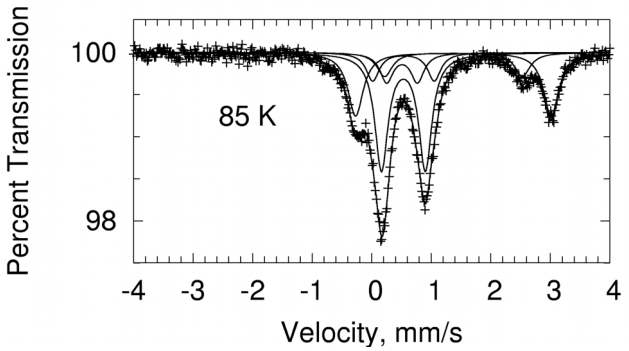

Fig. 2. Mössbauer spectrum of ferrorosemaryite from Rubindi, obtained at 85 K.

Table 1. Electron-microprobe analysis of ferrorosemaryite.

	1	2
P_2O_5	46.00(0.18)	2.981
Al_2O_3	9.12(0.19)	0.823
Fe_2O_3 (*)	21.01(1.50)	1.210
FeO (*)	11.10(1.55)	0.711
MgO	0.19(0.08)	0.022
MnO	7.96(0.23)	0.516
CaO	0.44(0.09)	0.036
Na_2O	2.85(0.35)	0.423
K_2O	0.01(0.01)	tr.
Total	98.68	

Analysts: F. Fontan and P. de Parseval. 1: Average of 9 analyses (in wt. %, with σ given in parentheses). 2: Number of cations based on 12 O per formula unit. (*): FeO and Fe_2O_3 were calculated from the Mössbauer spectrum.

the Mn^{2+} to Mn^{3+} transition is very high, and is comprised in the stability field of hematite (Norton, 1955; Huebner & Sato, 1970). Consequently, Fe^{2+} and Fe^{3+} can coexist with Mn^{2+} in the same mineral, but not with Mn^{3+}.

The empirical formula of ferrorosemaryite, deduced from the microprobe analyses (Table 1), corresponds to $\square_{1.00}(Na_{0.42}Mn^{2+}_{0.28}Ca_{0.04}\square_{0.26})_{\Sigma 1.00}(Fe^{2+}_{0.71}Mn^{2+}_{0.24}Fe^{3+}_{0.05})_{\Sigma 1.00}$ $Fe^{3+}_{1.00}(Al_{0.82}Fe^{3+}_{0.16}Mg_{0.02})_{\Sigma 1.00}[(P_{0.99}\square_{0.01})O_4]_3$. The simplified and idealised formula is $\square NaFe^{2+}Fe^{3+}Al(PO_4)_3$, which requires: P_2O_5 47.67, Al_2O_3 11.42, Fe_2O_3 17.88, FeO 16.09, Na_2O 6.94, total 100.00 wt. %.

Mössbauer spectroscopy

The iron-57 Mössbauer spectrum of ferrorosemaryite (Fig. 2) was recorded at 85 K on a constant acceleration spectrometer which used a rhodium matrix cobalt-57 source and was calibrated at 295 K with α-iron powder. The isomer shifts reported herein (Table 2) are relative to α-iron at 295 K. The Mössbauer spectral absorber contained 3.4 mg/cm² of powder.

The general appearance of the spectrum indicates that it should be fitted with at least three doublets, one assigned to Fe^{3+} and having a small isomer shift and quadrupole splitting, and two assigned to Fe^{2+} and having large isomer shifts and quadrupole splittings (Fig. 2). However, both the poor fits and the broad linewidths obtained from such preliminary fit reveal that a reasonable spectral fit will require at least three Fe^{3+} doublets and two Fe^{2+} doublets. Because preliminary fits have indicated that the linewidths of the three Fe^{3+} and the two Fe^{2+} doublets were identical within experimental error, final fit involved the adjustment of only 19 parameters: three Fe^{3+} fractions, two Fe^{2+} fractions, five isomer shifts, δ, five quadrupole splittings, ΔE_Q, two linewidths, Γ, as well as the total spectral area and spectral baseline. The hyperfine parameters, obtained from this final fit, are given in Table 2.

The less intense Fe^{2+} doublet, with the smaller quadrupole splitting value (2.3 mm/s), was assigned to Fe^{2+} on the M(2a) site, whereas the second Fe^{2+} doublet corresponds to Fe^{2+} on the M(1) site (Table 2). The values of isomer shift and quadrupole splitting for this doublet are in good agreement with those observed by Hatert *et al*. (2005) for Fe^{2+} on the M(1) site of the alluaudite-type compounds $Na_2(Mn_{1-x}Fe^{2+}_x)_2Fe^{3+}(PO_4)_3$ (x = 0.75 and 1.00).

Among the three Fe^{3+} doublets, that with the larger area was attributed to Fe^{3+} on the M(2b) site, and that with the larger quadrupole splitting value (1.03 mm/s) was attributed to Fe^{3+} on the M(1) site (Table 2). Larger quadrupole splitting values for Fe^{2+} on the M(1) site, compared to the values for Fe^{2+} on the M(2) site, were already observed by Hatert *et al*. (2005) in synthetic alluaudite-type compounds, and are due to the larger distortion of M(1), compared to M(2). This doublet assignment can be extended to ferrorosemaryite, because the morphologies of the M crystallographic sites are similar in the alluaudite and wyllieite structures.

Finally, it is important to note that the values of isomer shifts and quadrupole splittings, for Fe^{3+} on the M(2a) and M(2b) sites (Table 2), are in very good agreement with the values obtained for Fe^{3+} on the M(2) site of synthetic alluaudite-type compounds (Hermann *et al*., 2002; Hatert *et al*., 2003, 2004 and 2005).

Infrared spectroscopy

The infrared spectrum of ferrorosemaryite (Fig. 3) was recorded with a Nicolet NEXUS spectrometer, from 32 scans with a 1 cm^{-1} resolution, over the 400-4000 cm^{-1}

Table 2. Mössbauer spectral hyperfine parameters for ferrorosemaryite at 85 K.

Fe valence	Site assignment	δ (mm/s)*	ΔE_Q (mm/s)	Γ (mm/s)	Area (%)	Number of atoms *p.f.u.*
Fe^{3+}	M(1)	0.535(6)	1.03(3)	0.267(9)	10(2)	0.192
	M(2a)	0.51(3)	0.52(7)	0.267(9)	11(2)	0.211
	M(2b)	0.533(6)	0.74(2)	0.267(9)	42(3)	0.807
Fe^{2+}	M(2a)	1.37(6)	2.3(1)	0.311(8)	10(1)	0.192
	M(1)	1.372(3)	3.284(6)	0.311(8)	27(1)	0.519

* The isomer shifts are relative to room temperature α-iron powder.

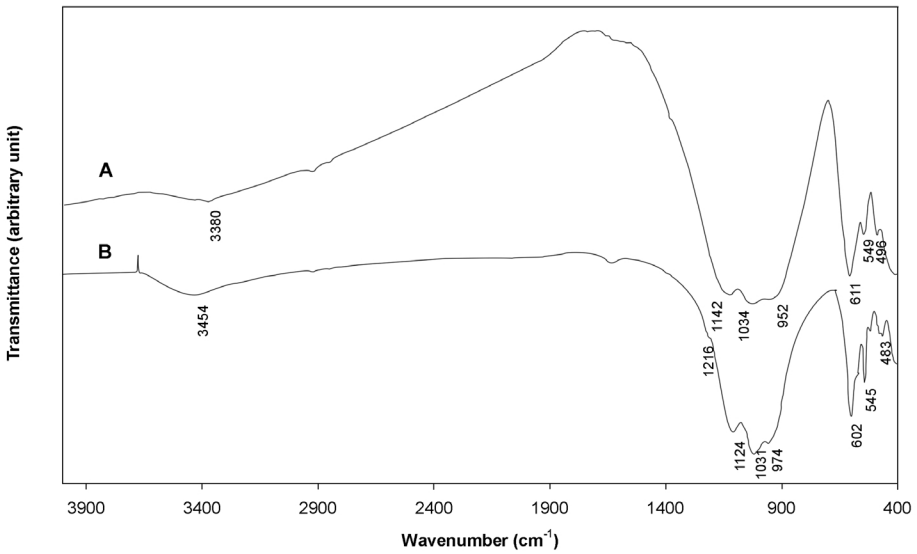

Fig. 3. Infrared spectrum of ferrorosemaryite from Rubindi (A), compared to that of alluaudite from Buranga, Rwanda (B).

region. The sample was prepared by intimately mixing 2 mg of sample with KBr in order to obtain a 150 mg homogeneous pellet which was subsequently dried for a few hours at 120°C. To prevent water contamination, the measurements were performed under a dry air purge.

Because the infrared spectra of wyllieite-type compounds exhibit a complexity which is related both to the low symmetry and to the large unit-cell of the wyllieite structure, it is difficult to assign all the individual absorption bands of the ferrorosemaryite spectrum. Nevertheless, the similarity between this spectrum and those of synthetic alluaudite-type compounds permits the assignments proposed by Antenucci *et al.* (1993) and Hatert *et al.* (2002, 2003 and 2005) to be used for ferrorosemaryite. According to these authors, the stretching vibrational modes of the PO_4 tetrahedra occur in the 1200-900 cm^{-1} region, whereas both the PO_4 bending vibrations, and the AlO_6 and FeO_6 stretching vibrational modes, contribute to the absorption between *ca.* 400 and 650 cm^{-1}. At lower frequencies is the domain of lattice vibrations.

It is important to note a large absorption band, localised at 3375 cm^{-1} (Figure 3), which is related to the O-H stretching vibrational mode (Farmer, 1974). The presence of protons in natural alluaudites has been suspected by

Table 3. Indexed powder X-ray diffraction pattern of ferrorosemaryite.

$I_{obs.}$	$d_{obs.}$ (Å)	$d_{calc.}$(Å)	*h k l*	$I_{obs.}$	$d_{obs.}$ (Å)	$d_{calc.}$(Å)	*h k l*
30	8.102	8.118	1 1 0	20	2.468	2.469	4 2 0
50	6.167	6.173	0 2 0	5	2.362	2.363	5 0 $\bar{1}$
40	5.382	5.387	2 0 0	5	2.295	2.296	1 5 $\bar{1}$
< 5	4.381	4.388	1 2 $\bar{1}$	5	2.197	2.198	3 3 1
5	4.122	4.120	1 1 1	5	2.152	2.152	1 3 2 ; 2 1 2
45	4.054	4.059	2 2 0	15	2.123	2.123	5 1 0
5	3.661	3.664	3 1 $\bar{1}$	15	2.050	2.050	3 1 $\bar{3}$; 5 3 $\bar{1}$
65	3.448	3.449	3 1 0	10	2.035	2.035	3 5 0 ; 5 2 0
5	3.350	3.343	0 3 1	5	1.970	1.970	4 4 $\bar{2}$
5	3.258	3.258	3 2 $\bar{1}$	5	1.950	1.951	5 3 $\bar{2}$
5	3.206	3.207	2 3 $\bar{1}$	5	1.933	1.933	1 5 $\bar{2}$
5	3.084	3.086	0 4 0	10	1.923	1.922	2 6 0
40	3.011	3.013	1 1 $\bar{2}$	15	1.910	1.909	5 3 0
10	2.914	2.914	2 2 1	5	1.877	1.876	5 4 $\bar{1}$
15	2.867	2.867	0 0 2	10	1.832	1.832	6 2 $\bar{2}$
20	2.821	2.820	3 1 $\bar{2}$	5	1.791	1.790	3 5 1
15	2.785	2.784	2 2 $\bar{2}$	5	1.771	1.771	5 1 1
75	2.693	2.694	4 0 0	10	1.719	1.719	3 3 2 ; 5 2 1
100	2.677	2.678	2 4 0	< 5	1.695	1.695	5 3 $\bar{3}$
5	2.641	2.643	2 4 $\bar{1}$	< 5	1.652	1.653	4 0 2
10	2.601	2.600	0 2 2	5	1.628	1.629	6 4 $\bar{2}$
5	2.561	2.558	4 0 $\bar{2}$	5	1.597	1.597	2 5 $\bar{3}$

Table 4. Experimental details for the single-crystal X-ray diffraction study of ferrorosemaryite.

Dimensions of the crystal (mm)	*ca.* 0.10 × 0.15 × 0.20
a (Å)	11.838(1)
b (Å)	12.347(1)
c (Å)	6.2973(6)
β (°)	114.353(6)
V (Å^3)	838.5(1)
Space group	$P2_1/n$
Diffractometer	Bruker P4
Operating conditions	50 kV, 30 mA
Radiation	Mo$K\alpha$ (λ = 0.71073 Å)
Scan mode	ω scan
Scan width (°)	0.75
Scan speed (°/min.)	10 to 60
$2\theta_{max}$	60°
Range of indices	$-15 \le h \le 15$, $-17 \le k \le 17$, $-8 \le l \le 8$
Measured intensities	5492
Unique reflections	2444
Independent non-zero [$F_o > 4\sigma(F_o)$] reflections	2072
Absorption correction	Semi-empirical
l.s. refinement program	SHELXL-93 (Sheldrick, 1993)
Refined parameters	184
R_1 (on *F*'s) ($F_o > 4\sigma(F_o)$)	0.0243
R_1 (all)	0.0300
wR_2 (all)	0.0704
S (goodness of fit)	1.082
Max Δ/σ in the last l.s. cycle	0.000
Max peak and hole in the final ΔF map (*e*/Å^3)	+0.64 and –0.60

Fransolet *et al.* (1994) on the basis of wet chemical analyses, and the synthetic protonated alluaudite-type compounds $M^+M^{2+}_3(PO_4)(HPO_4)_2$ (M^+ = Na, Ag; M^{2+} = Mn, Co) have been synthesised by Lii & Shih (1994), Leroux *et al*. (1995 a and b) and Guesmi & Driss (2002). The infrared spectrum of ferrorosemaryite does not show any supplementary absorption band around 1600 cm^{-1}, related to the bending vibrational mode of H_2O, thus demonstrating the absence of molecular water in the channels of the structure. Consequently, the band at 3375 cm^{-1} could be attributed to the stretching vibrations of OH-groups localised on the apex of HPO_4^{2-} tetrahedra.

Powder X-ray diffraction

The powder X-ray diffraction pattern of ferrorosemaryite, given in Table 3, was obtained on a PHILIPS PW-3710 diffractometer using Fe$K\alpha$ radiation (λ = 1.9373 Å). This powder pattern is similar to those of phosphates of the wyllieite group. On the basis of the *d*-spacings shown in Table 3, which were calibrated with an internal standard of $Pb(NO_3)_2$, the least-squares refinement program LCLSQ 8.4 (Burnham, 1991) has served to calculate the unit-cell parameters *a* = 11.824(2), *b* = 12.346(3), *c* = 6.293(1) Å, and β = 114.32(1)°.

Structure refinement

A crystal fragment of ferrorosemaryite (0.10 × 0.15 × 0.20 mm) was preliminarily tested by rotation and Weissenberg methods (Cu$K\alpha$ radiation, λ = 1.5418 Å). The unit-cell parameters, *a* = 11.73(3), *b* = 12.39(2), *c* = 6.32(3) Å, and β = 115°, correspond to those of alluaudite- and wyllieite-type phosphates. Systematic absences were in agreement with the $P2_1/n$ space group of the wyllieite structure.

The X-ray structural study was carried out on a Bruker P4 four-circle diffractometer (Mo$K\alpha$ radiation, λ = 0.71073 Å), using the same crystal fragment. The unit-cell parameters and standard deviations were calculated for the setting angles of 42 reflections with 9.8° < 2θ < 26.3°: *a* = 11.838(1), *b* = 12.347(1), *c* = 6.2973(6) Å, β = 114.353(6)°, and *V* = 838.5(1) Å^3. The intensities of 5492 reflections corresponding to 2444 unique reflections ($R_{int.}$ = 0.022) were measured by the ω scan technique in the range 3.3° < 2θ < 60° ($h = \overline{15} \rightarrow 15$, $k = \overline{17} \rightarrow 17$, $l = \overline{8} \rightarrow 8$). Data were corrected for Lorentz polarization and absorption effects, the latter with a semi-empirical method using a reliable set of ψ-scan data.

The crystal structure was refined in the $P2_1/n$ space group, which was confirmed from systematic absences, starting from the atomic coordinates of ferrowyllieite (Moore & Molin-Case, 1974). Cationic site occupancies were refined to obtain the better agreement with the chemical composition of ferrorosemaryite (Table 1). For the sake of simplicity, Ca and Mg, which occur in very low amounts, were not taken into account in the crystal structure refinement. Finally, the occupancy of Fe^{3+} against Al was refined in the M(2a) and M(2b) sites, the occupancy of Fe^{2+} against Na was refined in the M(1) site, the occupancy of Mn against Na was refined on the X(1a) site, and the occupancy of Na against vacancies was refined on the

Table 5. Final fractional coordinates and equivalent isotropic displacement parameters (Å²) for ferrorosemaryite.

Site	Atom	*x*	*y*	*z*	*Ueq*
X(1a)	Mn*	0.5	0	0	0.0267(3)
X(1b)	Na**	0.5	0	0.5	0.026(1)
M(1)	Fe***	0.00328(3)	0.26143(3)	0.26174(3)	0.0083(1)
M(2a)	Al****	0.28229(4)	-0.34426(4)	0.36563(8)	0.0060(2)
M(2b)	Fe*****	0.21847(3)	-0.14873(3)	0.62250(6)	0.0059(1)
P(1)	P	0.00302(4)	-0.28623(5)	0.24047(9)	0.0068(1)
P(2a)	P	0.24165(5)	-0.10219(4)	0.12096(9)	0.0071(1)
P(2b)	P	0.24473(5)	0.11152(4)	0.64403(9)	0.0067(1)
O(1a)	O	0.4481(1)	-0.2835(1)	0.5168(3)	0.0095(3)
O(1b)	O	0.4531(1)	-0.7119(1)	0.0427(3)	0.0089(3)
O(2a)	O	0.1081(1)	-0.3549(1)	0.2316(3)	0.0129(3)
O(2b)	O	0.0936(1)	-0.6337(1)	0.7439(3)	0.0122(3)
O(3a)	O	0.3186(2)	-0.3317(1)	0.0944(3)	0.0101(3)
O(3b)	O	0.3339(1)	-0.6612(1)	0.6140(3)	0.0102(3)
O(4a)	O	0.1227(2)	0.4024(1)	0.3394(3)	0.0139(3)
O(4b)	O	0.1154(1)	-0.3969(1)	0.7783(3)	0.0137(3)
O(5a)	O	0.2302(1)	-0.1721(1)	0.3171(3)	0.0111(3)
O(5b)	O	0.2224(1)	-0.8169(1)	0.8274(3)	0.0098(3)
O(6a)	O	0.3122(2)	-0.4902(1)	0.3835(3)	0.0129(3)
O(6b)	O	0.3117(2)	-0.4998(1)	0.8723(3)	0.0123(3)

Refined sites occupancies:
*0.366(9) Mn + 0.135(18) Na;
**0.190(4) Na + 0.310(4) □;
***0.911(8) Fe + 0.088(18) Na;
****0.708(19) Al + 0.296(9) Fe;
*****0.791(9) Fe + 0.215(19) Al.

X(1b) site. The refinement was completed using anisotropic displacement parameters for all atoms. The final conventional R_1 factor was 0.0243. Further details of the intensity data collection and refinement are given in Table 4.

Table 6. Selected bond distances (Å) and angles (°) for ferrorosemaryite.

P(1)-O(2a)	1.526(2)	X(1a)-O(4b) × 2	2.141(2)
P(1)-O(2b)	1.545(2)	X(1a)-O(2b) × 2	2.216(2)
P(1)-O(1a)	1.547(2)	X(1a)-O(4a) × 2	2.407(2)
P(1)-O(1b)	1.546(2)	Mean	**2.255**
Mean	**1.541**		
		X(1b)-O(2a) × 2	2.331(2)
O(2a)-P(1)-O(2b)	106.4(1)	X(1b)-O(4a) × 2	2.360(2)
O(2a)-P(1)-O(1a)	108.59(9)	X(1b)-O(4b) × 2	2.647(2)
O(2a)-P(1)-O(1b)	112.32(9)	X(1b)-O(2b) × 2	2.833(2)
O(2b)-P(1)-O(1a)	111.72(9)	Mean	**2.543**
O(2b)-P(1)-O(1b)	108.15(9)		
O(1a)-P(1)-O(1b)	109.62(9)	M(1)-O(4b)	2.131(2)
Mean	**109.47**	M(1)-O(1a)	2.132(2)
		M(1)-O(4a)	2.168(2)
P(2a)-O(6a)	1.518(2)	M(1)-O(1b)	2.174(2)
P(2a)-O(4a)	1.521(2)	M(1)-O(3b)	2.208(2)
P(2a)-O(5a)	1.557(2)	M(1)-O(3a)	2.239(2)
P(2a)-O(3b)	1.559(2)	Mean	**2.175**
Mean	**1.539**		
		M(2a)-O(6a)	1.831(2)
O(6a)-P(2a)-O(4a)	112.06(9)	M(2a)-O(2a)	1.883(2)
O(6a)-P(2a)-O(5a)	110.27(9)	M(2a)-O(3a)	1.932(2)
O(6a)-P(2a)-O(3b)	109.64(9)	M(2a)-O(1a)	1.945(2)
O(4a)-P(2a)-O(5a)	108.75(9)	M(2a)-O(5b)	1.985(2)
O(4a)-P(2a)-O(3b)	109.11(9)	M(2a)-O(5a)	2.199(2)
O(5a)-P(2a)-O(3b)	106.85(9)	Mean	**1.963**
Mean	**109.45**		
		M(2b)-O(6b)	1.876(2)
P(2b)-O(6b)	1.513(2)	M(2b)-O(3b)	2.003(2)
P(2b)-O(4b)	1.525(2)	M(2b)-O(5a)	2.006(2)
P(2b)-O(3a)	1.542(2)	M(2b)-O(1b)	2.018(2)
P(2b)-O(5b)	1.561(2)	M(2b)-O(2b)	2.037(2)
Mean	**1.535**	M(2b)-O(5b)	2.172(2)
		Mean	**2.019**
O(6b)-P(2b)-O(4b)	110.54(9)		
O(6b)-P(2b)-O(3a)	108.84(9)		
O(6b)-P(2b)-O(5b)	111.07(9)		
O(4b)-P(2b)-O(3a)	111.76(9)		
O(4b)-P(2b)-O(5b)	107.12(9)		
O(3a)-P(2b)-O(5b)	107.47(9)		
Mean	**109.47**		

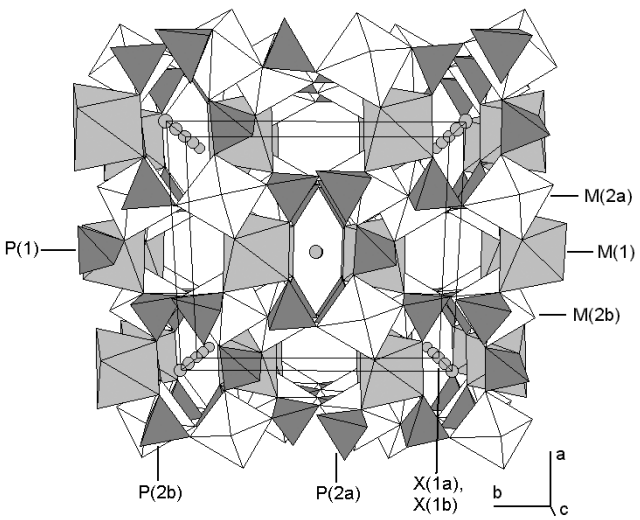

Fig. 4. Projection of the crystal structure of ferrorosemaryite. The PO_4 tetrahedra are densely shaded. The shaded M(1) octahedra are occupied by Fe^{2+} and Na, and the unshaded M(2a) and M(2b) octahedra are occupied by Fe^{3+} and Al, respectively. The circles indicate Na and Mn^{2+} on the X(1a) and X(1b) crystallographic sites.

Discussions

Compatibility index

The compatibility index of ferrorosemaryite is calculated with the relationship proposed by Mandarino (1981). The calculation of K_P was performed with the calculated density of 3.617 g/cm³. The compatibility index, 1-(K_P/K_C), is 0.019, and ranges in the category "superior" following Mandarino (1981).

Structural features

Final positional parameters for ferrorosemaryite are given in Table 5, whereas selected bond distances are reported in Table 6. Anisotropic displacement parameters can be obtained from the authors or through the EJM Editorial Office-Paris. The basic features of the crystal structure of ferrorosemaryite are identical to those of the other members of the wyllieite group. They consist of kinked chains of edge-sharing octahedra stacked parallel to {101}. These chains are formed by a succession of M(2a)-M(2b) octahedral pairs, linked by highly distorted M(1)

Table 7. Refined site populations (RSP, *apfu*), refined site-scattering values (RSS, *epfu*), mean bond-lengths (MBL, Å), assigned site populations (ASP, *apfu*), calculated site-scattering values (CSS, *epfu*), and calculated bond lengths (CBL, Å) for ferrorosemaryite.

	Results of the structure determination			**Results of the chemical analysis**		
Site	**RSP**	**RSS**	**MBL**	**ASP**	**CSS**	**CBL***
X(1a)	0.732 Mn + 0.270 Na	21.3	2.255	0.850 Mn^{2+} + 0.150 Na	22.9	2.259
X(1b)	0.380 Na	4.2	2.543	0.336 Na + 0.074 Mn^{2+} + 0.072 Ca	7.0	2.557
M(1)	0.911 Fe + 0.088 Na	24.7	2.175	0.568 Fe^{2+} + 0.198 Fe^{3+} + 0.180 Na + 0.054 Mn^{2+}	23.2	2.199
M(2a)	0.708 Al + 0.296 Fe	16.9	1.963	0.723 Al + 0.143 Fe^{2+} + 0.134 Fe^{3+}	16.6	1.985
M(2b)	0.791 Fe + 0.215 Al	23.4	2.019	0.878 Fe^{3+} + 0.100 Al + 0.022 Mg	24.4	2.036

*: The CBL have been calculated from the ASP, assuming a full occupancy for the X(1b) crystallographic site.

Table 8. Bond-valence table (vu) for ferrorosemaryite.

	X(1a)	**X(1b)**	**M(1)**	**M(2a)**	**M(2b)**	**P(1)**	**P(2a)**	**P(2b)**	**Σ**
O(1a)			0.360	0.485		1.208			2.05
O(1b)			0.322		0.480	1.212			2.01
O(2a)		0.255 *		0.574		1.279			2.11
O(2b)	0.318 *	0.066 *			0.456	1.215			2.06
O(3a)			0.270	0.502				1.225	2.00
O(3b)			0.293		0.500		1.170		1.96
O(4a)	0.190 *	0.236 *	0.327				1.296		2.05
O(4b)	0.389 *	0.109 *	0.361					1.282	2.14
O(5a)				0.244	0.496		1.176		1.92
O(5b)				0.435	0.317			1.163	1.92
O(6a)				0.650			1.307		1.97
O(6b)					0.705			1.325	2.03
Scalc.	1.79	1.33	1.93	2.90	2.96	4.91	4.95	5.00	
Stheor.	1.85	1.30	2.02	2.86	2.98	5.00	5.00	5.00	

The bond valences were calculated from the bond lengths given in Table 6, and from the assigned site populations of Table 7, with the parameters of Brown & Altermatt (1985). *: Bond valences were multiplied by two, for the calculation of the valence on the X crystallographic sites, and a full occupancy has been assumed for the X(1b) site.

octahedra (Fig. 4). Equivalent chains are connected in the *b* direction by the P(1), P(2a) and P(2b) phosphate tetrahedra to form sheets oriented perpendicular to [010]. These interconnected sheets produce channels parallel to *c*, channels that contain the large X sites.

It is important to note that the wyllieite structure is topologically similar to the alluaudite structure (Moore & Molin-Case, 1974). However, the ordering of cations in the wyllieite structure implies a splitting of the M(2) and X(1) sites of alluaudite into the M(2a) M(2b) and X(1a) X(1b) positions. Consequently, the *C*2/*c* space group of alluaudite transforms into $P2_1/n$ in wyllieite, with no significant change of the unit-cell parameters.

In the literature are present, besides an unpublished diploma thesis (Brier, 2000), only two crystal structure refinements reported on wyllieite-type compounds: one for ferrowyllieite (Moore & Molin-Case, 1974), and the second for qingheiite (Zhesheng *et al*., 1983). Compared to these minerals, Fe^{2+} on the M(2) sites is oxidised to Fe^{3+} in ferrorosemaryite, and its structure consequently contains an important number of vacancies per formula unit on the X sites. For this reason, the X(2) site is totally empty in ferrorosemaryite, and the X(1b) site contains 0.310 vacancies (Table 5). The morphology of the X(1a) site is shown in Fig. 5a, and corresponds to a very distorted octahedron, whereas the morphology of the X(1b) site (Fig. 5b) can be described as a very distorted cube. It is noteworthy to note that the morphology of X(1b) is similar to the morphology of the X(1) site of the alluaudite structure (Antenucci *et al*., 1995; Hatert *et al*., 2000).

Compared to the crystal structures of ferrowyllieite (Moore & Molin-Case, 1974) and qingheiite (Zhesheng *et al*., 1983), the data presented in this paper also indicate a

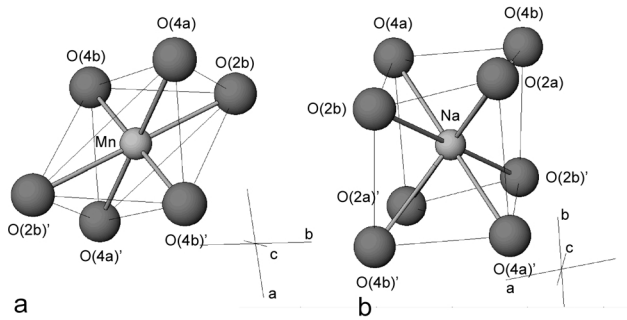

Fig. 5. Coordination polyhedra of the X(1a) (a) and X(1b) (b) crystallographic sites of ferrorosemaryite.

Table 9. Comparison of the physical properties of ferrorosemaryite with those of other minerals of the wyllieite group.

	Wyllieite	Ferrowyllieite	Rosemaryite	Ferrorosemaryite	Qingheiite
References	1	2, 3	1	4	5
Space group	$P2_1/n$	$P2_1/n$	$P2_1/n$	$P2_1/n$	$P2_1/n$
a (Å)	11.967(2)	11.868(15)	11.977(2)	11.824(2)	11.856(3)
b (Å)	12.462(3)	12.382(12)	12.388(2)	12.346(3)	12.411(3)
c (Å)	6.409(1)	6.354(9)	6.320(1)	6.293(1)	6.421(1)
β (°)	114.63(2)	114.52(8)	114.45(2)	114.32(1)	114.45(2)
X	Colourless	Smoky bluish-grey	Brownish yellow	Dark green	Dark bluish green
Y	Greenish blue	Smoky bluish-green	Brownish yellow	Dark green to brownish	Jade green
Z	Greenish blue	Green	Greenish yellow	Dark brown	Light yellowish green
α	1.685(2)	1.688(2)	1.723(2)	1.730(5)	1.678
β	1.688(2)	1.691(2)	1.742(2)	1.758(7)	1.684
γ	1.692(2)	1.696(2)	1.758(2)	1.775(5)	1.691
Optical sign	+	+	-	-	+
2V (°)	90	50	80	82(1)	79.6
Dispersion	n.g.	r < v strong	n.g.	r < v strong	r > v strong
D_{meas} (g/cm³)	n.g.	3.601(3)	n.g.	n.g.	3.718
D_{calc} (g/cm³)	n.g.	3.60	n.g.	3.62	3.61

1. Fransolet (1995); 2. Moore & Ito (1973); 3. Moore & Molin-Case (1974); 4. This study; 5. Zhesheng *et al.* (1983); n.g. : not given.

different distribution of Fe^{3+} and Al between the M(2a) and M(2b) crystallographic sites. In ferrowyllieite and qingheiite, the M(2b) site is mainly occupied by Al, whereas Fe^{2+} or Mg are located on the M(2a) site. This distribution is confirmed by the mean M(2b)-O bond lengths (1.973 and 2.001 Å), which are significantly shorter than the mean M(2a)-O bond lengths (2.098 and 2.092 Å). In contrast, the ferrorosemaryite structure contains mainly Al on the M(2a) site, whereas the M(2b) site is occupied by Fe^{3+} (Table 5). This distribution, which is confirmed by the M(2a)-O and M(2b)-O bond distances (Table 6), does not correspond to that proposed by Moore & Ito (1979) for wyllieite-type phosphates.

Taking into account the results of the microprobe analyses, of the Mössbauer spectral study, and of the single-crystal structure refinement, a more detailed cationic distribution has also been established. Table 7 shows that the refined site populations (RSP), obtained from the single-crystal structure refinement (Table 5), are in good agreement with the assigned site populations (ASP), which take into account the chemical results. The assigned Fe populations on the M crystallographic sites (Table 7) are close to the values deduced from the Mössbauer spectral results (Table 2), and the refined site scattering values (RSS) and mean bond lengths (MBL), obtained from the structure refinement, are close to the calculated site scattering values (CSS) and calculated bond lengths (CBL), respectively (Table 7). This confirms again the reliability of the final assigned site populations.

Finally, the bond valence table for ferrorosemaryite is presented in Table 8, where the bond valence sums were calculated according to the equation $s = \exp[(R_0 - R)/0.37]$, with the R_0 values of Brown & Altermatt (1985). The bond valences for O and P atoms are very close to the theoretical values of 2.00 and 5.00, respectively (Table 8). Concerning the cationic sites, a very good correspondence between the theoretical and the calculated values is generally observed.

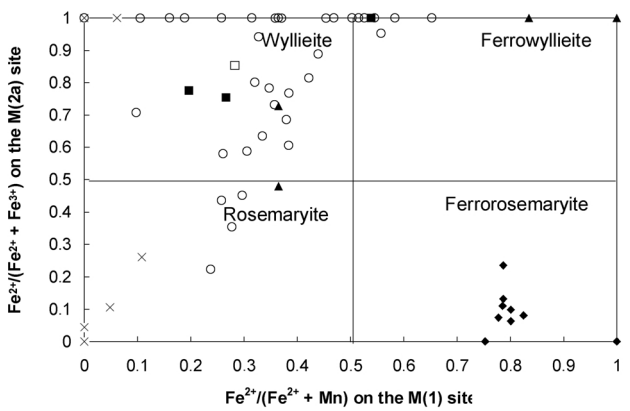

Fig. 6. Nomenclature of the wyllieite group of minerals. Chemical analyses of ferrorosemaryite from Rubindi are shown on this diagram (diamonds), as well as the analyses of wyllieites, ferrowyllieites, and rosemaryites given by Moore & Ito (1979) (triangles), Ek & Nysten (1990) (squares), Corbella & Melgarejo (1990) (open square), Fransolet (1995) (crosses), and Roda *et al.* (1996) (circles).

Ferrorosemaryite in the wyllieite group of minerals

In granitic pegmatites, particularly in the beryl-columbite-phosphate subtype of the rare-element pegmatites (Černý, 1991), wyllieite-type phosphates display chemical compositions ranging from $Na_2(Mn,Fe^{2+})Fe^{2+}Al(PO_4)_3$ to $\square Na(Mn,Fe^{2+})Fe^{3+}Al(PO_4)_3$, with K^+, Ca^{2+} or Mn^{2+} replacing Na^+ on the X(2), X(1a) and X(1b) sites, Li^+, Mg^{2+} or Zn^{2+} replacing iron on the M(2a) site, and Mg^{2+} or Fe^{3+} replacing Al^{3+} on the M(2b) site, where $\square$ represents a lattice vacancy. The crystal chemistry of these phosphates has been investigated in detail by Moore & Ito (1979), who proposed a revision of their nomenclature. According to these authors, the

name wyllieite corresponds to $Na_2MnFe^{2+}Al(PO_4)_3$, whereas the name rosemaryite designates the more oxidised composition, $\square NaMnFe^{3+}Al(PO_4)_3$. The prefix ferro- is then added if Fe^{2+} prevails in the M(1) site, thus leading to ferrowyllieite, $Na_2Fe^{2+}{}_2Al(PO_4)_3$ (Moore & Ito 1979), and to ferrorosemaryite, $\square NaFe^{2+}\ Fe^{3+}Al(PO_4)_3$, described herein. The name qingheiite has been introduced by Zhesheng *et al*. (1983) for the Mg-rich equivalent of wyllieite, $Na_2MnMgAl(PO_4)_3$. The transition from wyllieite to rosemaryite corresponds to the substitution mechanism $Na^+ + Fe^{2+} \rightarrow \square + Fe^{3+}$, which takes place during the oxidation processes affecting the pegmatites (Fransolet, 1995).

A comparison of the physical properties of ferrorosemaryite, with those of other minerals of the wyllieite group, is shown in Table 9. It is interesting to compare the greenish-blue colour of wyllieite and ferrowyllieite, and the brownish to yellowish colour of oxidised rosemaryite and ferrorosemaryite. Similar colours were already observed for minerals of the alluaudite group, for example in the Kibingo pegmatite, Rwanda, where primary hagendorfite exhibits a greenish to bluish colour, whereas oxidised alluaudite exhibits a yellowish to brownish colour (Fransolet *et al*., 2004).

The nomenclature of the Fe-Mn-bearing phosphate minerals of the wyllieite group is shown in Fig. 6, which is based on the occupancies of the M(2) and M(1) crystallographic sites (Moore & Ito, 1979). The microprobe analyses of wyllieite-type phosphates, available in the literature (Moore & Ito, 1979; Ek & Nysten, 1990; Corbella & Melgarejo, 1990; Fransolet, 1995; Roda *et al*., 1996), have been plotted on this diagram. Because the Mössbauer spectra and structure refinements were not given in these publications, the Fe^{2+}/Fe^{3+} ratio was calculated in order to maintain the charge balance, and the cations were distributed on the M(2) and M(1) sites according to their effective ionic radii (Shannon, 1976). Despite these simplifications, it must be pointed out that all the analyses of the sample from the Rubindi pegmatite occur into the compositional field of ferrorosemaryite, and that no other analysis from the literature shows a composition of ferrorosemaryite.

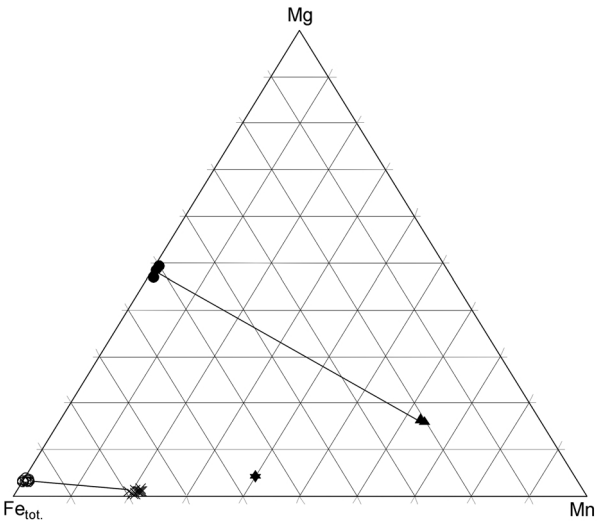

Fig. 7. Mg-Fe-Mn diagram showing the chemical compositions of ferrorosemaryite and scorzalite from Rubindi (crosses and empty circles, respectively), compared to wyllieite and scorzalite from Hålsjöberg (Ek & Nysten, 1990; triangles and filled circles, respectively). The star represents the composition of ferrowyllieite from Hålsjöberg (Ek & Nysten, 1990).

Distinction between alluaudite- and wyllieite-type phosphates

The distinction between alluaudite- and wyllieite-type phosphates can be made on the basis of the microprobe analysis, but the final confirmation of the structure-type requires the identification of the space group. The powder X-ray diffraction pattern can be useful for the identification, because some additional lines of low intensity can be observed in wyllieite-type compounds, lines which are not compatible with the *C*-centered space group of alluaudite. These lines were observed by Fransolet (1995) on the powder pattern of rosemaryite from Buranga, Rwanda. However, a first visual examination of the powder pattern of ferrorosemaryite does not show the presence of these supplementary lines, because of their very low intensities. For this reason, the powder X-ray diffraction pattern of ferrorosemaryite is very similar to those of alluaudite-type phosphates.

Consequently, the identification of wyllieite-type phosphates can only be confirmed by the use of single-crystal X-ray diffraction techniques, such as the precession camera, the Weissenberg camera, or the 4-circle diffractometer, in order to confirm the $P2_1/n$ space group. Even the infrared spectra are similar for alluaudite- and wyllieite-type compounds (Fig. 3), despite the more ordered cationic distribution in the wyllieite structure.

Genetic considerations

In the Rubindi pegmatite, ferrorosemaryite appears in close association with scorzalite. This scorzalite is Fe-rich, with a $Fe_{tot}/(Fe_{tot}+Mg)$ ratio of 0.97, similar to the $Fe_{tot}/(Fe_{tot}+Mg)$ ratio of associated ferrorosemaryite, that is 0.99. Ek & Nysten (1990) also observed wyllieite in association with scorzalite in the Hålsjöberg and Hökensås kyanite deposits, Sweden. As in Rubindi, the $Fe_{tot}/(Fe_{tot}+Mg)$ ratios are very similar for these two phosphates (Fig. 7), thus indicating partitioning coefficients close to 1.00. Ek & Nysten (1990) also described ferrowyllieite from the same locality (Fig. 7), but in this case, this mineral was not associated with scorzalite.

Finally, the enrichment in Fe observed in the Rubindi pegmatite, which is responsible for the crystallization of ferrorosemaryite, indicates that this pegmatite is less evolved than the Buranga pegmatite, which contains rosemaryite (Fransolet, 1995). The occurrence of ferrorosemaryite also indicates a high crystallization temperature, since it is well known for alluaudites and for triphylites, for example, that the Fe-rich members in the solid solutions

crystallize at higher temperatures than the Mn-rich members (Černý *et al.*, 1996; Hatert, 2002 and 2004).

Acknowledgements: The comments of J. Mandarino and of an anonymous reviewer were greatly appreciated. Many thanks are also due to Ph. de Parseval, for the precious help during the microprobe analyses, to O. Medenbach, who measured accurately the 2*V* angle of ferrorosemaryite, and to F. Grandjean, who accepted to read the first version of the manuscript. F.H. and A.M.F. acknowledge the Fonds National de la Recherche Scientifique, Belgium, for a position of "Chargé de Recherches" and for the grant 1.5.112.02, respectively.

References

Antenucci, D., Miehe, G., Tarte, P., Schmahl, W.W., Fransolet, A.-M. (1993): Combined X-ray Rietveld, infrared and Raman study of a new synthetic variety of alluaudite, $NaCdIn_2(PO_4)_3$. *Eur. J. Mineral.*, **5**, 207-213.

Antenucci, D., Fransolet, A.-M., Miehe, G., Tarte, P. (1995): Synthèse et cristallochimie de $NaCaCdMg_2(PO_4)_3$, phosphate nouveau à structure alluaudite sans cation trivalent. *Eur. J. Mineral.*, **7**, 175-181.

Brier, M. (2000): Röntgenographische Kristallstrukturbestimmung zur Elementverteilung in Mischkristallen der Alluaudit-Wyllieit-Gruppe. Unpublished Diploma thesis, University of Stuttgart, 171 p.

Brown, I.D. & Altermatt, D. (1985): Bond-valence parameters obtained from a systematic analysis of the inorganic crystal structure database. *Acta Cryst*., **B41**, 244-247.

Burnham, C.W. (1991): LCLSQ version 8.4, last-squares refinement of crystallographic lattice parameters. Dept. of Earth & Planetary Sciences, Harvard University, 24 p.

Černý, P. (1991): Rare-element granitic pegmatites. Part I: Anatomy and internal evolution of pegmatite deposits. *Geosci. Canada*, **18(2)**, 49-67.

Černý, P., Ercit, T.S., Vanstone, P.T. (1996): Petrology and mineralization of the Tanco rare-element pegmatite, Southeastern Manitoba – Field trip guidebook A4, Geological Association of Canada/Mineralogical Association of Canada Annual Meeting, Winnipeg, Manitoba, May 27-29, 1996, 63 p.

Corbella, M. & Melgarejo, J.C. (1990): Características y distribución de los fosfatos de las pegmatitas graníticas de la peninsula del Cap de Creus (Pirineo oriental catalán). *Bol. Soc. Española Mineral.*, **13**, 169-182.

Daltry, D. C. & Von Knorring, O. (1998): Type-mineralogy of Rwanda with particular reference to the Buranga pegmatite. *Geologica Belgica*, **1**, 9-15.

Domergue, C., Fontan, F., Hérail, G. (1989): Les techniques artisanales d'exploitation des gîtes alluviaux: analogies dans le temps et dans l'espace. *Chron. Rech. Min.*, **497**, 131-138.

Ek, R. & Nysten, P. (1990): Phosphate mineralogy of the Hålsjöberg and Hökensås kyanite deposits. *Geol. För. Stockholm För.*, **112(1)**, 9-18.

Farmer, V.C. (1974): The infrared spectra of minerals. Mineralogical Society Monographs, **4**, 539 p.

Fransolet, A.-M. (1989): The problem of Na-Li substitution in primary Li-Al phosphates: new data on lacroixite, a relatively wide-spread mineral. *Can. Mineral.*, **27**, 211-217.

— (1995): Wyllieite et rosemaryite dans la pegmatite de Buranga, Rwanda. *Eur. J. Mineral*., **7**, 567-575.

Fransolet, A.-M., Antenucci, D., Fontan, F., Keller, P. (1994): New relevant data on the crystal chemistry, and on the genetical problem of alluaudites and wyllieites. *Abstracts of the 16th IMA general meeting, Pisa*, 125-126.

Fransolet, A.-M., Hatert, F. & Fontan, F., (2004): Petrographic evidence for primary hagendorfite in an unusual assemblage of phosphate minerals, Kibingo granitic pegmatite, Rwanda. *Can. Min.*, **42**, 697-704.

Guesmi, A. & Driss, A. (2002): $AgCo_3PO_4(HPO_4)_2$. *Acta Cryst*., **C58**, i16-i17.

Hatert, F. (2002): Cristallochimie et synthèse hydrothermale d'alluaudites dans le système Na-Mn-Fe-P-O: contribution au problème de la genèse de ces phosphates dans les pegmatites granitiques. Unpublished Ph. D. Thesis, University of Liège, 247 p.

— (2004): Etude cristallochimique et synthèse hydrothermale des alluaudites: contribution nouvelle au problème génétique des phosphates de fer et de manganèse dans les pegmatites granitiques et, partant, à celui de l'évolution de ces gisements. *Mém. Acad. royale Sci. Belgique, Cl. Sci., Coll. in-8°, 3ème série*, **XXI**, 96 p.

Hatert, F., Keller, P., Lissner, F., Antenucci, D. , Fransolet, A.-M. (2000): First experimental evidence of alluaudite-like phosphates with high Li-content: the $(Na_{1-x}Lix)MnFe_2(PO_4)_3$ series (x = 0 to 1). *Eur. J. Mineral.*, **12**, 847-857.

Hatert, F., Antenucci, D., Fransolet, A.-M., Liégeois-Duyckaerts, M. (2002): The crystal chemistry of lithium in the alluaudite structure: a study of the $(Na_{1-x}Lix)CdIn_2(PO_4)_3$ solid solution (x = 0 to 1). J. Solid State *Chem*., **163**, 194-201.

Hatert, F., Hermann, R.P., Long, G.J., Fransolet, A.-M., Grandjean, F. (2003): An X-ray Rietveld, infrared, and Mössbauer spectral study of the $NaMn(Fe_{1-x}Inx)_2(PO_4)_3$ alluaudite-like solid solution. *Am. Mineral*., **88**, 211-222.

Hatert, F., Long G.J., Hautot, D., Fransolet, A.-M., Delwiche, J., Hubin-Franskin, M.J. Grandjean, F. (2004): A structural, magnetic, and Mössbauer spectral study of several Na-Mn-Fe-bearing alluaudites. *Phys. Chem. Mineral.*, **31**, 487-506.

Hatert, F., Rebbouh, L., Hermann, R.P., Fransolet, A.-M., Long, G.J., Grandjean, F. (2005): Crystal chemistry of the hydrothermally synthesized $Na_2(Mn_{1-x}Fe^{2+}_x)_2Fe^{3+}(PO_4)_3$ alluaudite-type solid solution. *Am. Mineral.*, **90**, 653-662.

Hermann, R. P., Hatert, F., Fransolet, A.-M., Long, G. J., Grandjean, F. (2002): Mössbauer spectral evidence for next-nearest neighbour interactions within the alluaudite structure of $Na_{1-x}LixMnFe_2(PO_4)_3$. *Solid State Sci*., **4**, 507-513.

Huebner, J.S. & Sato, M. (1970): The oxygen fugacity-temperature relationships of manganese and nickel oxide buffers. *Am. Mineral.*, **55**, 934-952.

Lefèvre, P. (2003): Contribution à l'étude minéralogique et pétrographique des associations des phosphates d'aluminium des pegmatites de Rubindi et Kabilizi (Rwanda). Unpublished Diploma thesis, University of Liège, 58 p.

Leroux, F., Mar, A., Payen, C., Guyomard, D., Verbaere, A., Piffard, Y. (1995a): Synthesis and structure of $NaMn_3(PO_4)(HPO_4)_2$, an unoxidized variant of the alluaudite structure type. *J. Solid State Chem.*, **115**, 240-246.

Leroux, F., Mar, A., Guyomard, D., Piffard, Y. (1995b): Cation substitution in the alluaudite structure type : synthesis and structure of $AgMn_3(PO_4)(HPO_4)_2$. *J. Solid State Chem.*, **117**, 206-212.

Lii, K.-H. & Shih, P.-F. (1994): Hydrothermal synthesis and crystal structures of $NaCo_3(PO_4)(HPO_4)_2$ and $NaCo_3(AsO_4)(HAsO_4)_2$: synthetic modifications of the mineral alluaudite. *Inorg. Chem.*, **33**, 3028-3031.

Mandarino, J.A. (1981): The Gladstone-Dale relationship: Part IV. The compatibility concept and its application. *Can. Mineral.*, **19**, 441-450.

Moore, P.B. & Ito, J. (1973): Wyllieite, $Na_2Fe^{2+}{}_2Al(PO_4)_3$, a new species. *Mineral. Rec.*, **4**, 131-136.

Moore, P.B. & Ito, J. (1979): Alluaudites, wyllieites, arrojadites: crystal chemistry and nomenclature. *Mineral. Mag.*, **43**, 227-235.

Moore, P.B. & Molin-Case, J. (1974): Contribution to pegmatite phosphate giant crystal paragenesis: II. The crystal chemistry of wyllieite, $Na_2Fe^{2+}{}_2Al(PO_4)_3$, a primary phase. *Am. Mineral.*, **59**, 280-290.

Norton, F.J. (1955): Dissociation pressures of iron and copper oxides. *General Electric Research Laboratory Report*, 55-R1-1248.

Roda, E., Fontan, F., Pesquera, A., Velasco, F. (1996): The phosphate mineral association of the granitic pegmatites of the Fregeneda area (Salamanca, Spain). *Mineral. Mag.*, **60**, 767-778.

Shannon, R.D. (1976): Revised effective ionic radii and systematic studies of interatomic distances in halides and chalcogenides. *Acta Cryst.*, **A32**, 751-767.

Sheldrick, G.M. (1993): SHELXL93. Program for the Refinement of Crystal Structures. University of Göttingen, Germany.

Varlamoff, N. (1963): Les phénomènes de greisenification, d'albitisation et de lépidolitisation et leurs relations spatiales avec les granites et les pegmatites granitiques d'Afrique. *Ann. Soc. Géol. Belgique*, **86**, B285-322.

Varlamoff, N. (1975): Classification des gisements d'étain. *Acad. Roy. Sci. Outre-Mer*, *Cl. Sci. nat. médic.*, **XIX-5**, 1-64.

Von Knorring, O. (1970): Mineralogical and geochemical aspects of pegmatites from orogenic belts of equatorial and southern Africa. *in* "African magmatism and tectonics", T.N. Clifford and I.G. Gass, eds. Oliver & Boyd, Edinburgh, 157-184.

Zhesheng, M., Nicheng, S., Zhizhong, P. (1983): Crystal structure of a new phosphatic mineral-quingheiite. *Sci. Sinica*, *série B*, **XXVI(8)**, 876-884.

Received 4 February 2005
Modified version received 18 April 2005
Accepted 13 May 2005